ChemPubSoc Europe

DOI: 10.1002/open.201600116

Open Access ChemistryOPEN Full Papers

Synthesis and Comparative Catalytic Study of Zirconia–$MnCO_3$ or –Mn_2O_3 for the Oxidation of Benzylic Alcohols

Mohamed E. Assal,[a] Mufsir Kuniyil,[a] Mujeeb Khan,[a] Abdulrahman Al-Warthan,[a] Mohammed Rafiq H. Siddiqui,[a] Wolfgang Tremel,[b] Muhammad Nawaz Tahir,*[b] and Syed Farooq Adil*[a]

We report on the synthesis of the zirconia–manganese carbonate **ZrO_x(x%)–$MnCO_3$** catalyst (where $x = 1$–7) that, upon calcination at 500 °C, is converted to zirconia–manganese oxide **ZrO_x(x%)–Mn_2O_3**. We also present a comparative study of the catalytic performance of the both catalysts for the oxidation of benzylic alcohol to corresponding aldehydes by using molecular oxygen as the oxidizing agent. **ZrO_x(x%)–$MnCO_3$** was prepared through co-precipitation by varying the amounts of $Zr(NO_3)_4$ (w/w%) in $Mn(NO_3)_2$. The morphology, composition, and crystallinity of the as-synthesized product and the catalysts prepared upon calcination were studied by using scanning electron microscopy, transmission electron microscopy, energy-dispersive X-ray spectroscopy, and powder X-ray diffraction. The surface areas of the catalysts [133.58 $m^2 g^{-1}$ for **ZrO_x(1%)–$MnCO_3$** and 17.48 $m^2 g^{-1}$ for **ZrO_x(1%)–Mn_2O_3**] were determined by using the Brunauer–Emmett–Teller method, and the thermal stability was assessed by using thermal gravimetric analysis. The catalyst with composition **ZrO_x(1%)–$MnCO_3$** precalcined at 300 °C exhibited excellent specific activity (48.00 $mmol g^{-1} h^{-1}$) with complete conversion within approximately 5 min and catalyst cyclability up to six times without any significant loss in activity. The specific activity, turnover number and turnover frequency achieved is the highest so far (to the best of our knowledge) compared to the previously reported catalysts used for the oxidation of benzyl alcohol. The catalyst showed selectivity for aromatic alcohols over aliphatic alcohols.

1. Introduction

One of the global challenges is to reduce the emission of greenhouse gases while increasing the industrial production/efficiency to meet the society needs. Especially, the petrochemical industry is at the focus of environmental pollution. Therefore, the development and synthesis of ecofriendly, low-cost, and efficient catalysts for the petrochemical industry are inevitable.

Among the chemical transformations, selective oxidation is an important chemical reaction, which plays an essential role in the preparation of many chemicals on an industrial and at the laboratory scale.[1] One very important application of the oxidation reactions in petrochemicals is the synthesis of aldehydes by oxidation of the corresponding alcohols. Aldehydes play a vital role as the starting material for many industrial and pharmaceutical formulations.[2] Among the different catalysts reported for the oxidation reactions, metal-supported metal oxides or mixed metal oxides (MMO) have gained much attention, such as Au NPs–Ce–SnO for the preparation of benzaldehyde from benzyl alcohol,[3] Pt–CeO_2/C and Pt–TiO_2/C as electrocatalysts for methanol oxidation, or TiO_2 (001) nanosheets for the oxidation of benzyl alcohol.[4] CoCuO MMO microspheres have been used for the oxidation of ethylbenzene,[5] the electrochemical oxidation of glucose, and the selective oxidation of 5-hydroxymethyl furfural, to name only a few.[6] MMOs containing manganese received significant attention as catalysts for various applications including oxidation reactions, manganese titanium oxide hydroxide-supported palladium nanoparticles being an example for the electro-oxidation of methanol,[7] and for the removal of Cr^{VI} from aqueous solutions.[8] Fe_3O_4 and MnO_2 assembled on halloysite nanotubes have been used for the electrochemical detection of mercury(II) ions,[9] MnO_2 films and MnO_2 nanosheets decorated with NiO nanoparticles as efficient supercapacitor electrode materials,[10] and $MnCo_2O_4$@C nanoparticles as a catalyst for water splitting.[11] Manganese-promoted Ce–Al–Si is a catalyst for the oxidation of acetone,[12] $Pd_mMn_{1-m}O_x$ nanoparticle-decorated graphene or graphene-based composite photocatalysts have

[a] M. E. Assal, M. Kuniyil, Dr. M. Khan, Prof. A. Al-Warthan, Prof. M. R. H. Siddiqui, Dr. S. F. Adil
Department of Chemistry, College of Science
King Saud University
P.O. Box 2455, Riyadh 11451 (Kingdom of Saudi Arabia)
E-mail: sfadil@ksu.edu.sa

[b] Prof. W. Tremel, Dr. M. Nawaz Tahir
Institute of Inorganic and Analytical Chemistry
Johannes Gutenberg-University of Mainz
55128 Mainz (Germany)
E-mail: tahir@uni-mainz.de

The ORCID identification number(s) for the author(s) of this article can be found under http://dx.doi.org/10.1002/open.201600116.

© 2016 The Authors. Published by Wiley-VCH Verlag GmbH & Co. KGaA. This is an open access article under the terms of the Creative Commons Attribution-NonCommercial-NoDerivs License, which permits use and distribution in any medium, provided the original work is properly cited, the use is non-commercial and no modifications or adaptations are made.

catalyzed the oxidation of alcohol,[13] and copper manganese oxide nanoparticles have been used for the oxidation of carbon monoxide,[14] alcohols,[15] and various hydrocarbons.[14,16] Similarly, MMOs containing manganese oxide along with those that are noble-metal doped/supported[16i,17] are also used for the oxidation of benzyl alcohol.

Similarly, zirconia-based catalysts are used for the oxidation reaction, as an example ZrO_2–CeO_2/SiO_2[18] or gold supported on Zr doped ceria catalysts have been employed for the oxidation of CO,[19] Ru–Cu/ZrO_2 as glycerol hydrogenolysis catalysts,[20] and Cu–Ni/ZrO_2 for the synthesis of diethyl carbonate from CO_2 and ethanol. A polyoxometalate–zirconia (POM/ZrO_2) nanocomposite[21] has been reported for the selective oxidation of alcohols in the liquid phase.[19,22] Zirconia-supported CrO_3[22b] or ruthenium-supported on a CaO–ZrO_2[22c] have been used for the oxidation of alcohols to aldehydes, whereas zirconium-based metal–organic frameworks have been employed for the photocatalytic oxidation of alcohol under visible light.[22d] Zirconia-supported sodium decatungstate ($Na_4W_{10}O_{32}$/ZrO_2)[22a] led to the formation of carboxylic acids.

However, there are few reports for manganese (Mn)- and zirconium (Zr)-based MMOs as catalysts. Also, $MnCO_3$, which is low cost, environmentally friendly, and transforms to manganese oxides[18] upon heating, has been used as a raw material to prepare manganese-oxide-based catalysts. However, $MnCO_3$ as a pure phase or mixed with other metal oxides is not studied as an oxidation catalyst. In this contribution, we report the synthesis of **ZrO_x(*x*%)–$MnCO_3$** (where $x = 1$–7), followed by calcination at elevated temperature to prepare **ZrO_x(*x*%)–Mn_2O_3**. Both catalysts were studied for the oxidation of benzylic alcohols to the corresponding aldehydes. The catalysts were prepared by co-precipitation with varying the amounts of $Zr(NO_3)_4$ (w/w%) and $Mn(NO_3)_2$ (Scheme 1). The morphology, composition, and phase composition of the as-synthesized catalyst and those of the catalyst after calcination were monitored by using scanning electron microscopy (SEM), transmission electron microscopy (TEM), energy-dispersive X-ray (EDX) spectroscopy, powder X-ray diffraction (XRD), Brunauer–Emmett–Teller (BET), and thermal gravimetric analysis (TGA). The catalytic efficiency for the oxidation of various aromatic alcohols was evaluated by using gas chromatography.

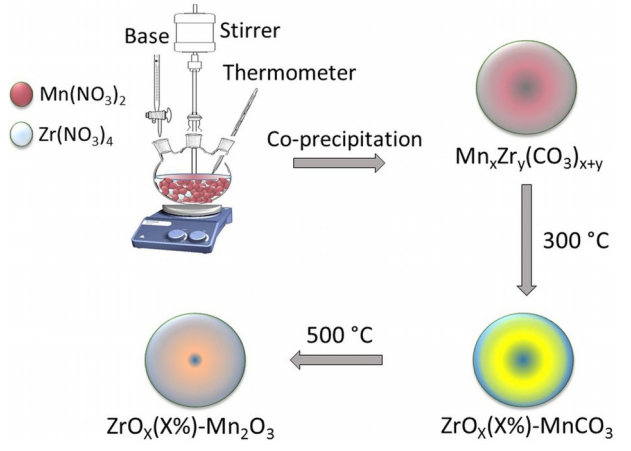

Scheme 1. Synthetic representation of **ZrO_x–$MnCO_3$** followed by calcination at 500 °C to prepare **ZrO_x–Mn_2O_3**.

2. Results and Discussion

2.1. Characterization of the Catalysts

2.1.1. Morphology and Phase Structure

The catalyst obtained by co-precipitation was calcined at 300 and 500 °C. The SEM images of the as-synthesized catalyst **ZrO_x(1%)–$MnCO_3$**, and the products calcined at temperatures 300 °C **[ZrO_x(1%)–$MnCO_3$]** or 500 °C **[ZrO_x(1%)–Mn_2O_3]** are shown in Figure 1. The SEM images show particles with a well-defined cuboidal morphology. The particle-size distribution (Figures 1C and 1F, obtained with the Image J program) shows only slight variations in the particle sizes with changes in calcination temperature. The composition of the catalyst is determined by using EDX and stays within experimental error to the theoretical composition (Table 1).

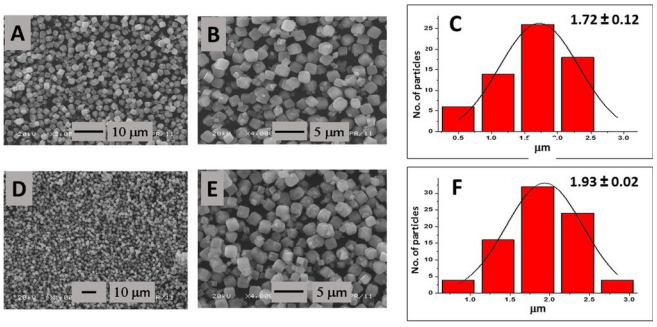

Figure 1. SEM analysis of the synthesized catalysts calcined at A–C) 300 °C; D–F) 500 °C. A) Overview image for as-synthesized **ZrO_x(1%)–$MnCO_3$** and B) **ZrO_x(1%)–$MnCO_3$**. C) Size distribution of **ZrO_x(1%)–$MnCO_3$**, D) overview image for as synthesized **ZrO_x(1%)–Mn_2O_3** and E) **ZrO_x(1%)–Mn_2O_3**, and F) size distribution of **ZrO_x(1%)–Mn_2O_3**.

Table 1. Elemental composition of the catalyst **ZrO_x(1%)–MnO** calcined at different temperatures.

Calcination temperature [°C]	Mass [%] Element				Compound		
	C	O	Mn	Zr	C	MnO	ZrO_2
300	29.97	15.84	53.24	0.95	29.97	68.75	1.28
500	22.72	17.5	58.36	1.43	22.72	75.36	1.93

The XRD patterns for the as-synthesized catalysts (uncalcined) (Figure 2a) show the presence of rhodochrosite, *syn*-manganese carbonate (JCPDS No. 00-007-0268) with space group *R*-3c (167), which, upon calcination at 300 °C, transformed to rhodochrosites manganese carbonate oxides (JCPDS No. 00-001-0981) [space group *R*-3c (167)] (Figure 2b).

Calcination at 500 °C led to the formation of bixbyite Mn_2O_3 (JCPDS No.:00-002-0909) (Figure 2c). The reflections marked

© 2017 The Authors. Published by Wiley-VCH Verlag GmbH & Co. KGaA, Weinheim

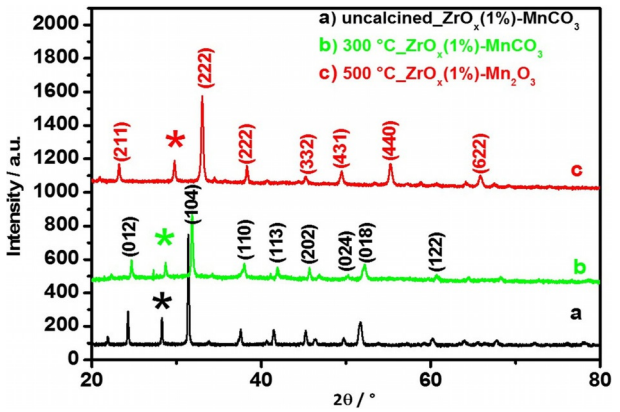

Figure 2. XRD pattern of the catalyst at different temperatures a) uncalcined rhodochrosite, *syn*-manganese carbonate (JCPDS No. 00-007-0268), b) at 300 °C **ZrO$_x$(1 %)–MnCO$_3$** transformed to rhodochrosites manganese carbonate oxides (JCPDS No. 00-001-0981), and c) at 500 °C converted to bixbyite Mn_2O_3 (JCPDS No.:00-002-0909). The reflections marked with an asterisk (*) could be attributed to the presence of ZrO_x (monoclinic phase for uncalcined and at 300 °C calcined and tetragonal for sample calcined at 500 °C).

with * could be attributed to the presence of ZrO_x (monoclinic phase for uncalcined and 300 °C-calcined samples, and tetragonal for 500 °C-calcined sample).

The HRTEM images of **ZrO$_x$(1 %)–MnCO$_3$** nanoparticles obtained after calcination at 300 and 500 °C (Figures 3a and 3b) show polycrystalline particles with clear lattice fringes. The interplanar distance was calculated from the HRTEM image of the sample calcined at 300 °C (Figure 3a), which revealed *d* spacings of 0.29 and 0.23 nm, corresponding to the (104) and the (110) planes of rhombohedral $MnCO_3$. For the sample calcined at 500 °C (Figure 3b), the most prominent lattice spacing corresponds to the (200) plane of α-Mn_2O_3.

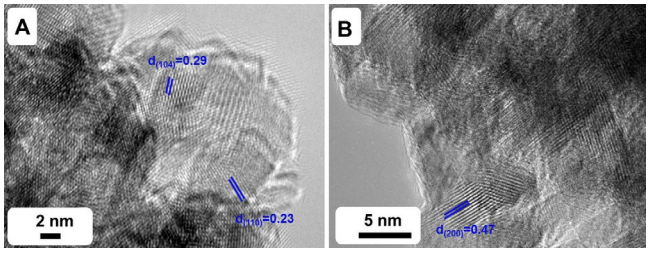

Figure 3. HRTEM analysis of the catalysts calcined at a) 300 °C and b) 500 °C.

2.1.2. Thermal Stability

The thermal stability of **ZrO$_x$(1 %)–MnCO$_3$** calcined at 300 °C or **ZrO$_x$(1 %)–Mn$_2$O$_3$** obtained after calcining at 500 °C catalysts was determined by using TGA (Figures 4a and 4b). The catalyst calcined at 300 °C was stable up to 410 °C with a small weight loss of < 8 % (attributed to physisorbed moisture). Increasing the temperature led to an additional weight loss of 15 % in the temperature range between 410 and 610 °C, corresponding to the decarboxylation of $MnCO_3$ to form $MnO_2 + CO_2$ and further oxidation of MnO_2 to Mn_2O_3 (O_2:4 MnO_2/2 $Mn_2O_3 + O_2$), as reported by Zhu et al.[1] These findings are in agreement with the results (5 % weight loss) obtained for heating the catalysts calcined at 500 °C.

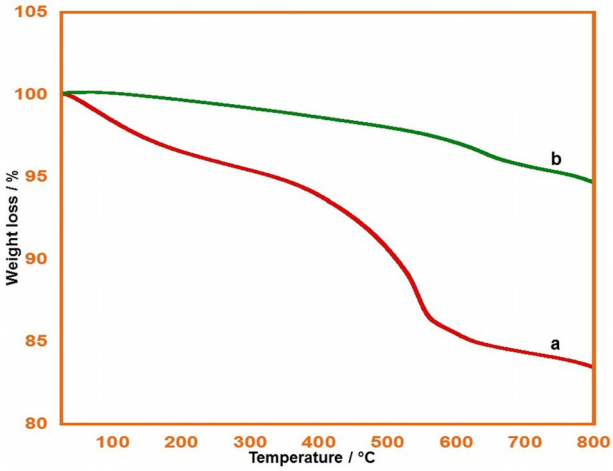

Figure 4. TGA curve of **ZrO$_x$(1 %)–MnCO$_3$** calcined at 300 °C and 500 °C: a) **ZrO$_x$(1 %)–MnCO$_3$** and b) **ZrO$_x$(1 %)–Mn$_2$O$_3$**.

2.1.3. Surface-Area Measurements

The surface area of the prepared catalysts was determined by using BET sorption measurements. The catalyst calcined at 300 °C [**ZrO$_x$(1 %)–MnCO$_3$**] has the highest surface area (133.58 $m^2 g^{-1}$), whereas the surface are of the catalyst calcined at 500 °C [**ZrO$_x$(1 %)–Mn$_2$O$_3$**] was severely reduced (17.48 $m^2 g^{-1}$), owing to sintering. It is worth mentioning that sintering not only results inter-particles, but it also minimizes the porosity within a single particle. The results are compiled in Table 2.[23] The catalytic activity of **ZrO$_x$(1 %)–MnCO$_3$** may be correlated to the activity surface area (vide infra).

Table 2. Effect of calcination temperature on the catalytic properties.[a]

Entry	Catalyst	*T* [°C]	Surface area [$m^2 g^{-1}$]	Conversion [%]	Selectivity [%]	Specific activity [mmolg^{-1} h^{-1}]	*TON*	*TOF* [h^{-1}]
1	**ZrO$_x$(1 %)–MnCO$_3$**	300	133.58	100.00	< 99	13.33	82.14	164.27
2	**ZrO$_x$(1 %)–Mn$_2$O$_3$**	500	17.48	21.53	< 99	2.87	17.68	35.37

[a] Reaction conditions: amount of catalyst 300 mg, reaction temperature 100 °C, oxygen flow rate 20 mL min^{-1}, benzyl alcohol 2 mmol, toluene 10 mL, and reaction time 30 min.

© 2017 The Authors. Published by Wiley-VCH Verlag GmbH & Co. KGaA, Weinheim

2.2. Catalytic Evaluation

To investigate the catalytic performance of the prepared catalysts and to compare the catalytic activity of **ZrO_x(1%)–$MnCO_3$** and **ZrO_x(1%)–Mn_2O_3**, both catalysts underwent testing for the oxidation of benzyl alcohol to benzaldehyde as a model reaction. To check the effect of ZrO_x, the activity of phase-pure $MnCO_3$ and Mn_2O_3 was tested under identical experimental conditions for comparison.

2.2.1. Effect of Calcination Temperature

As the calcination temperature may play an essential role for the kinetics of the reaction,[24] the obtained catalysts were evaluated for the oxidation of benzyl alcohol. The catalyst calcined at 300 °C [**ZrO_x(1%)–$MnCO_3$**] yielded a 100% conversion of benzaldehyde with 13.33 $mmolg^{-1}h^{-1}$ specific activity and 164.27 h^{-1} turnover frequency (*TOF*), within 30 min of the reaction, whereas the catalyst calcined at 500 °C [**ZrO_x(1%)–Mn_2O_3**] yielded a 21.53% conversion within the first 30 min (Figure 5)

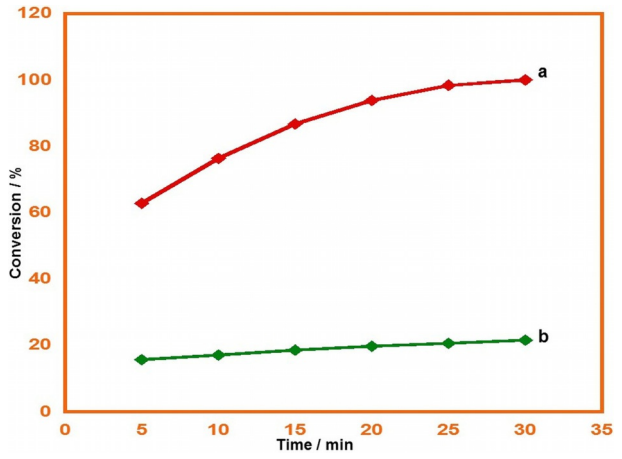

Figure 5. Graphical representation of benzyl alcohol oxidation using catalyst calcined at a) 300 °C and b) 500 °C.

with 2.87 $mmolg^{-1}h^{-1}$ specific activity and 35.37 h^{-1} *TOF* (Table 2). This shows that the presence of ZrO_x on $MnCO_3$ plays an important role during the oxidation reaction, whereas ZrO_x-supported Mn_2O_3 obtained upon calcination at 500 °C displays the lowest catalytic performance and specific activity. This may be related to a decomposition of the active catalyst phase or reduction in surface area (as mentioned above), whereas the sample calcined at 300 °C has $MnCO_3$ oxides with active sites to promote catalysis. These catalytic activity results also correlate with results obtained from the surface area analysis, which revealed that the **Zr(1%)–$MnCO_3$** catalyst synthesized at 300 °C possesses the highest surface area, whereas the other calcination temperature results in the depreciation of surface area (Table 2). The specific activity, turnover number (*TON*), and *TOF* were found to decrease with increasing calcination temperature. The benzyl alcohol conversion, specific activity, *TON*, *TOF* and selectivity obtained over the catalyst are listed in Table 2.

2.2.2. Effect of the Amount of ZrO_x Promotor

To investigate the optimum amount of ZrO_x present in $MnCO_3$ to effect the kinetics of the reaction, catalysts prepared by varying the amount of ZrO_x precursor from 1 to 7% were tested for the oxidation of benzyl alcohol to benzaldehyde. All catalysts were calcined at 300 °C, and the reaction was performed at 100 °C. **ZrO_x(1%)–$MnCO_3$** showed a complete conversion of benzyl alcohol. The specific activity for this conversion is 13.33 $mmolg^{-1}h^{-1}$ and the *TOF* was 64.27 h^{-1}. **ZrO_x(3%)–$MnCO_3$**, **ZrO_x(5%)–$MnCO_3$**, and **ZrO_x(7%)–$MnCO_3$** led to 95.25, 61.49, and 40.25% conversion, respectively. To ascertain the presence of ZrO_x as the promoter, a catalyst prepared without ZrO_x was subjected to catalytic evaluation under a similar set of conditions. A 82.55% benzyl alcohol conversion along with specific activity of 11.0 $mmolg^{-1}h^{-1}$ was achieved, which clearly indicates the promotion effect of ZrO_x in the catalyst with 1 and 3% ZrO_x. The specific activity, *TON*, and *TOF* were found to decrease with increased percentage presence of ZrO_x in the catalyst. Further increasing the ZrO_x content led to a decrease in the catalytic performance, which may be attributed to a blocking of active sites or to an agglomeration of zirconia, as indicated by the results of the BET analysis. The graphical representation is given in Figure 6.

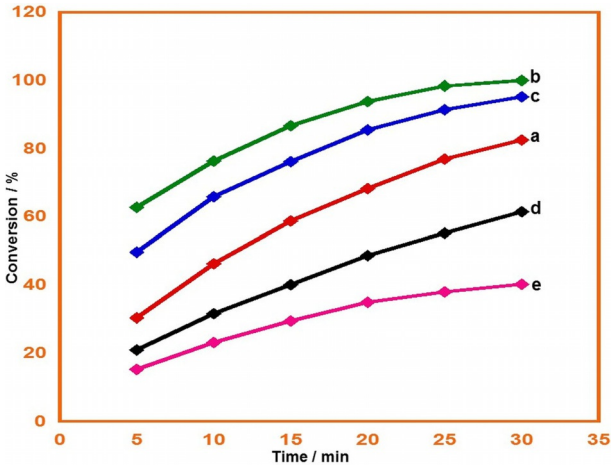

Figure 6. Graphical representation of benzyl alcohol oxidation using catalyst a) **$MnCO_3$**, b) **ZrO_x(1%)–$MnCO_3$**, c) **ZrO_x(3%)–$MnCO_3$**, d) **ZrO_x(5%)–$MnCO_3$**, and e) **ZrO_x(7%)–$MnCO_3$**.

The specific activity for the conversions decreased from 12.70 to 5.37 $mmolg^{-1}h^{-1}$ with no change in selectivity towards benzaldehyde for all reactions. The benzyl alcohol conversion, specific activity, and selectivity obtained for all catalyst are compiled in Table 3.

2.2.3. Effect of Amount of Catalyst

To determine the effect of the amount of catalyst on the catalytic performance, the amount of the **ZrO_x(1%)–$MnCO_3$** catalyst was varied (100, 200, 300, 400, and 500 mg), while the reaction conditions [temperature (100 °C), molecular oxygen as

© 2017 The Authors. Published by Wiley-VCH Verlag GmbH & Co. KGaA, Weinheim

Table 3. Effect on the catalytic properties by weight% of ZrO_x in the catalyst.[a]

Entry	ZrO_x [%]	Conversion [%]	Selelctivity [%]	Specific activity [mmolg^{-1}h^{-1}]	*TON*	*TOF* [h^{-1}]
1	0	82.55	<99	11.00	–	–
2	1	100.00	<99	13.33	82.14	164.27
3	3	95.25	<99	12.70	26.08	52.16
4	5	61.49	<99	8.20	10.08	20.16
5	7	40.25	<99	5.37	4.74	9.47

[a] Reaction conditions: catalyst **ZrO_x(x%)–$MnCO_3$**, amount of catalyst 300 mg, calcination temperature 300 °C, reaction temperature 100 °C, oxygen flow rate 20 mL min^{-1}, benzyl alcohol 2 mmol, toluene 10 mL, and reaction time 30 min.

oxidant], and reaction time (5 min) were kept constant. The reaction carried out using 500 mg catalyst yielded a 100% conversion product within 5 min (Table 4, entry 5), whereas the conversion for the remaining samples was <100% within the same period of time. A 28.47% conversion was obtained with 100 mg of catalyst (Table 4, entry 1). The specific activity for this conversion was calculated to be 68.32 mmolg^{-1}h^{-1}. However, when the amount of catalyst was increased to 200, 300, 400, and 500 mg, the specific activity decreased to 53.89, 50.24, 48.74, and 48.00 mmolg^{-1}h^{-1}, respectively (Table 4, entries 2–5). The selectivity remained unchanged throughout the studies. The conversion of benzyl alcohol to benzaldehyde increased by increasing the amount of catalyst, whereas the specific activity decreased. A linear relationship can be deduced between the amount of catalyst and conversion of benzyl alcohol, as shown in Figure 7, and the catalytic results are compiled in Table 4.

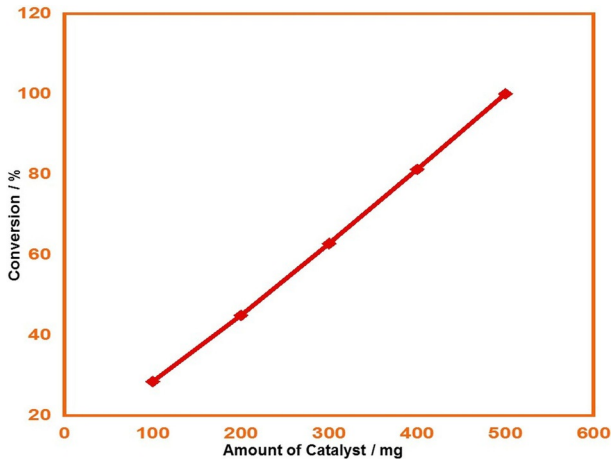

Figure 7. Effect on the conversion of benzyl alcohol to benzaldehyde by varying amount of the catalyst (mg). Reaction conditions: catalyst **ZrO_x(1%)–$MnCO_3$**, reaction temperature 100 °C, oxygen flow rate 20 mL min^{-1}, benzyl alcohol 2 mmol, toluene 10 mL, and reaction time 5 min.

2.2.4. Effect of Reaction Temperature

Figure 8 shows the effect of reaction temperature on the catalytic activity of the **ZrO_x(1%)–$MnCO_3$** catalyst for the oxidation of benzyl alcohol. Upon increasing the reaction temperature from 20 to 100 °C, the conversion of benzyl alcohol with the synthesized catalyst increased from 49.84 to 100%. The specific activity, *TON*, and *TOF* were found to increase with increased reaction temperature (Table 5).

It is worth mentioning that, when the reaction was carried out in the absence of a catalyst and otherwise a similar set of reaction conditions, no conversion product (i.e. benzaldehyde) was formed. To rule out the formation of benzaldehyde by oxidation of the solvent (toluene), a reaction was performed without the substrate (benzyl alcohol), and again no conversion product (benzaldehyde) was formed.

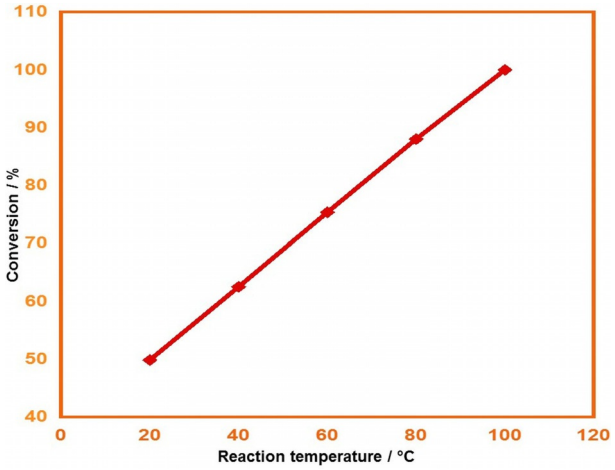

Figure 8. Effect of reaction temperature (°C) on the conversion of benzyl alcohol. Reaction conditions: catalyst **ZrO_x(1%)–$MnCO_3$**, oxygen flow rate 20 mL min^{-1}, benzyl alcohol 2 mmol, toluene 10 mL, and reaction time 5 min.

Table 4. Influence of amount the catalyst on the conversion product.[a]

Entry	Catalyst amount [mg]	Time [min]	Conversion [%]	Selectivity [%]	Specific activity [mmolg^{-1}h^{-1}]	*TON*	*TOF* [h^{-1}]
1	100	5	28.47	<99	68.32	70.12	841.44
2	200	5	44.91	<99	53.89	55.34	664.08
3	300	5	62.8	<99	50.24	51.59	619.08
4	400	5	81.23	<99	48.74	50.05	600.60
5	500	5	100	<99	48.00	49.29	591.48

[a] Reaction conditions: catalyst **ZrO_x(1%)–$MnCO_3$**, reaction temperature100 °C, oxygen flow rate 20 mL min^{-1}, benzyl alcohol 2 mmol, and toluene 10 mL.

© 2017 The Authors. Published by Wiley-VCH Verlag GmbH & Co. KGaA, Weinheim

Table 5. Effect of reaction temperature on the kinetics of the reaction.[a]

Entry	*T* [°C]	Conversion [%]	Selectivity [%]	Specific activity [mmolg^{-1} h^{-1}]	*TON*	*TOF* [h^{-1}]
1	20	49.84	<99	23.92	11.80	141.60
2	40	62.51	<99	30.0	30.81	369.72
3	60	75.36	<99	36.17	37.14	445.68
4	80	88.03	<99	42.25	43.39	520.68
5	100	100.00	<99	48.0	49.29	591.48

[a] Reaction conditions: catalyst **ZrO_x(1%)–$MnCO_3$**, amount the catalyst 500 mg, oxygen flow rate 20 mLmin^{-1}, benzyl alcohol 2 mmol, toluene 10 mL, and reaction time 5 min.

The specific activity and *TOF* of the catalyst were calculated and compared (Table 6) with the catalysts reported previously for the oxidation of benzyl alcohol to benzaldehyde.[16a,21,25] **ZrO_x(1%)–$MnCO_3$** showed 48 mmolg^{-1} h^{-1} as the highest specific activity and a *TOF* of 591.48 h^{-1} for benzyl alcohol oxidation. The specific activity for the oxidation of benzy alcohol using a copper/copper oxide nanoparticles supported on SBA-15 reported (Cruz et al.)[25a] in the aqueous phase (43.8 mmolg^{-1} h^{-1}, 73% conversion and 54% selectivity after 30 min) is significantly lower than the specific activity obtained for **ZrO_x(1%)–$MnCO_3$** [48 mmolg^{-1} h^{-1} for **ZrO_x(1%)–$MnCO_3$** with complete conversion and <99 selectivity in ca. 5 min] in the present study. Undecamolybdophosphate PMo_{11}-supported ZrO_2 led to a specific activity of 39.50 mmolg^{-1} h^{-1}, and only 23.7% of benzyl alcohol was converted to benzaldehyde with a selectivity of 92.3%.[25b] In summary, **ZrO_x(1%)–$MnCO_3$** calcined at 300 °C exhibited an excellent catalytic activity compared to all other catalysts listed in Table 6.

The exact mechanism can be postulated only by using in situ spectroscopic techniques. However, based on very established literature in the field, we propose the following mechanism for **ZrO_x–$MnCO_3$** or **ZrO_x–Mn_2O_3** (ZrO_x = 1–7 w/w%) catalyst-based oxidation of benzyl alcohol. In most of cases, the dehydrogenation step acts as the rate-limiting step in the oxidation of alcohols.[26] Moreover, the presence of a promoter (normally a base or catalyst support acting as solid base) can help to activate the O–H bond of alcohol to increase the oxidation. Here, in this catalytic system, ZrO_x dispersed on $MnCO_3$ acts as the promotor (basic sites ZrO_x).[27] $MnCO_3$ in the presence of molecular oxygen oxidized easily to high-valent Mn; most likely to γ-MnOOH,[28] and the organic molecule oxidizes at the expense of these high-valent Mn active sites. As reported by Tang et al.,[25j] and verified by others; we also believe that the oxidation mechanism follows the Mar–van Krevenlen-type mechanism. The active species is possibly O^{2-} and likely involves the transfer of two electrons in a single step. As the mechanism involves the exchange of oxygen from the lattices, the activity is very much dependent on the Mn–O bond strength in a MnO_x catalyst. This is the reason that, in our case,

Table 6. A comparison between our result and earlier reported results in the literature for the oxidation of benzyl alcohol to benzaldehyde.

Catalyst	Conversion [%]	Selectivity [%]	*T* [°C]	Reaction time [min]	*TOF* [h^{-1}]	Specific activity [mmolg^{-1} h^{-1}]	Ref.
ZrO_x(1%)–$MnCO_3$	100	<99	100	5	591.48	48.00	zhis work
Cu/IMIL-SBA-15-G1	73	54	80	30	66.0	43.80	[25a]
PMo_{11}/ZrO_2. Al_2O_3	23.7	92.3	90	1440	492.25	39.50	[25b]
CuZnO	<99	<99	RT	180	48.31	33.33	[25c]
Ru/CaO–ZrO_2	100	100	90	45	224.0	22.22	[22c]
2 Au/1CuO–ZnO	94	<99	RT	60	–[a]	18.80	[25d]
RHAC–CoPor	97.1	97.7	70	300	176.9	24.27	[29]
$CuMn_2$ oxide	100	<99	102	80	2.83	15.00	[30]
POM/ZrO_2	93	<99	25±5	240	–[a]	12.40	[21]
$Au^{(0)}$–zeolite	<95	<99	80	300	11.0	0.63	[31a]
CuMn oxide	100	<99	102	35	1.54	11.43	[15]
Mn–Fe–HD	53.9	70.6	94	300	–[a]	11.21	[25e]
MnO_2/GO (10/100)	98.1	100	110	240	1.17	1.23	[32]
AgNPs/GOSH + NHPI	61	58	80	1440	5.72	5.08	[25f]
5%Ag–MnO_2–5%Au	100	<99	100	90	13.55	4.44	[17e]
1%Ag–MnO_2	100	<99	100	120	35.97	3.33	[17d]
$CuAl_2O_4$	99	98	80	480	–[a]	1.25	[25g]
$CoAl_2O_4$	90.98	86.95	80	480	–[a]	1.14	[25h]
AuPd–6% GO/TiO_2	88.9	69.0	120	120	41.0	–[a]	[33]
Au-100CeO_2@SBA-15	18	<99	90	10	270.0	27.0	[34]
2% Au/HT-3	57.41	93.82	40	1440	9.61	0.96	[25i]
10% Mn/γ-Al_2O_3-p	93	<99	100	240	0.50	0.93	[25j]
EBTPPCC	96	–[a]	RT	80	–[a]	0.87	[25k]
In_2S_3	41.5	41.4%	hν	240	–[a]	0.65	[25l]
Au/1%CuO–3%MCM	73.0	94.3	80	1200	7.40	0.86	[35]
CoPc	97	83.5	50	180	194.0	–[a]	[36]
cell–$Pd^{(0)}$	100	82	80	900	22.22	0.22	[25m]
MnO_x/MCM-41	94	99	80	720	–[a]	0.026	[16a]
Pd(TOP)/MB-H_2O_2	28.7	<99	80	1440	36.15	0.30	[37]

[a] Calculation could not be carried out, owing to insufficient data provided in the literature article.

© 2017 The Authors. Published by Wiley-VCH Verlag GmbH & Co. KGaA, Weinheim

the ZrO_x–$MnCO_3$-based catalyst is more active where the surface Mn is oxidized to γ-MnOOH by molecular oxygen and acts more as a catalytic site than ZrO_x–Mn_2O_3.

The catalyst reusability is an important parameter used to define the significance of the catalyst from commercial point of view. In order to evaluate the re-usability and the stability, the ZrO_x(1 %)–$MnCO_3$ was subjected to the oxidation reaction, separated from the reaction mixture by centrifugation, washed with toluene several times and dried at 100 °C for 4 h to avoid contamination with reactant or product of the previous reaction and re-used up to six times, yielding the same conversion product and selectivity. However, there is an only a slight reduction in catalytic performance (Figure 9).

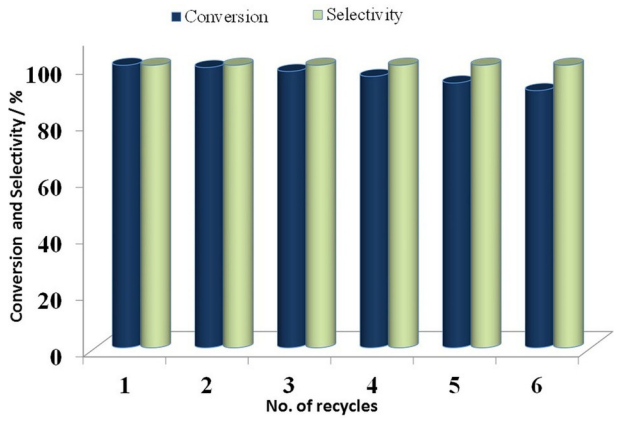

Figure 9. Graphical illustration of conversion product and selectivity obtained upon catalyst reuse.

2.3. Catalytic Performance on Substituted Benzyl Alcohol

Detailed catalytic parameters for the conversion of benzyl alcohol revealed that the best results obtained were achieved by using ZrO_x(1 %)–$MnCO_3$ after calcination at 300 °C, 2 mmol benzyl alcohol, 0.5 g catalyst, 10 mL toluene, 20 mL min^{-1} oxygen flow rate, and 100 °C reaction temperature. The oxidation of the other substituted alcohols (benzylic alcohols or citronellol) with substituents like 4-CH_3, 3-CH_3, 2-CH_3, 4-OCH_3, 3-OCH_3, 2,3,4-TriOMe, 4-Br, 4-Ph, 4-Cl, 2-Cl, 2,4-DiCl, 4-NO_2, 3-NO_2, 2-NO_2, 4-OH, 4-$C(CH_3)_3$, 4-CF_3, 4-F, and 2,3,4,5,6-pentafluoro groups (Table 7) were tested using the above-mentioned conditions. All benzylic alcohols and citronellol are completely converted to corresponding aldehydes. A >99% selectivity toward aldehydes is achieved in all reactions, and no other products are found. Benzyl alcohols containing electron-donating groups were observed to be the most reactive and exhibited shorter oxidation times, whereas benzylic alcohol substituted with electron-withdrawing groups was less reactive.[38] The increase in the catalytic performance for with electron-donating groups is probably caused by the adequate electron density at the active center compared to substrates containing electron-withdrawing groups. For instance, benzyl alcohol with electron-donating groups in the *para* positions (4-methoxylbenzyl alcohol) completely converted into the corresponding aldehyde after 5 min (Table 7, entry 3). Conversely, *para*-nitro-

Table 7. Selective oxidation of benzyl alcohol and its derivatives into corresponding aldehydes catalyzed by the ZrO_x(1 %)–$MnCO_3$ catalyst.[a]

Reaction no.	Reactant	Product	Time [min]	Conversion [%]	Selectivity [%]
1	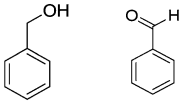		5	100	>99
2	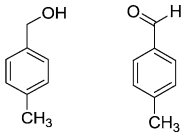		5	100	>99
3	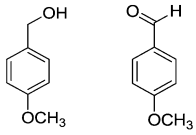		5	100	>99
4	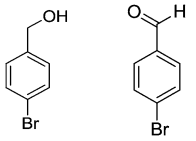		5	100	>99
5	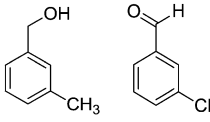		5	100	>99
6	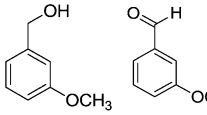		6	100	>99
7	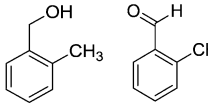		6	100	>99
8	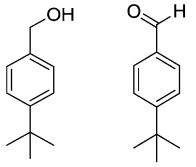		6	100	>99
9	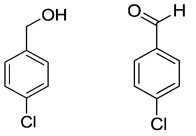		6	100	>99
10	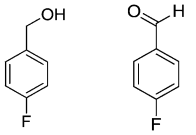		6	100	>99
11	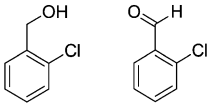		7	100	>99
12	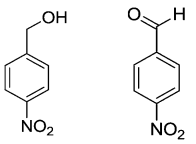		7	100	>99

© 2017 The Authors. Published by Wiley-VCH Verlag GmbH & Co. KGaA, Weinheim

Table 7. (Continued)

Reaction no.	Reactant	Product	Time [min]	Conversion [%]	Selectivity [%]
13	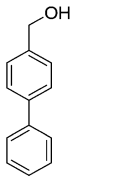	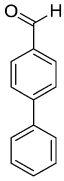	7	100	> 99
14	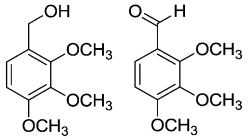		8	100	> 99
15	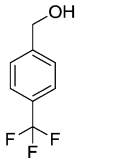	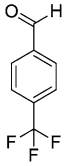	8	100	> 99
16	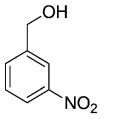	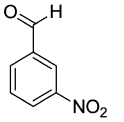	8	100	> 99
17	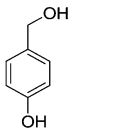	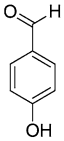	9	100	> 99
18	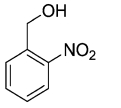	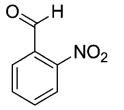	13	100	> 99
19	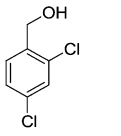	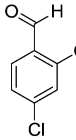	14	100	> 99
20	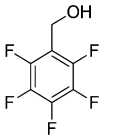	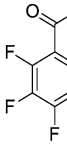	17	100	> 99
21	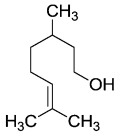	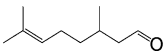	90	100	> 99

[a] Reaction conditions: calcination temperature 300 °C, amount the catalyst 500 mg, oxygen flow rate 20 mL min^{-}, alcohol 2 mmol, toluene 10 mL, and reaction temperature 100 °C.

benzyl alcohol, containing a *para*-electron-withdrawing group, required a longer reaction time (7 min) (Table 7, entry 12). On the other hand, it was reported that alcohols with substituents at the *para*-position exhibited a higher conversion than alcohols substituted in *meta* or *ortho* positions, because *para* substituents have lower steric hindrance.[39] For example, *para*-nitrobenzyl alcohol was fully oxidized to the corresponding aldehyde within 7 min (Table 7, entry 12), whereas *meta*- and *ortho*-nitrobenzyl alcohol were completely converted into the corresponding aldehydes after 8 and 13 min, respectively (Table 7, entries 16 and 18). Additionally, steric hindrance is an essential factor affecting the catalytic activity for the oxidation reactions. Thus, bulky groups such as 2,3,4-TriOMe, $-C(CH_3)_3$, $-CF_3$, 2,4-DiCl, and 2,3,4,5,6-pentafluoro attached to the phenyl ring reduced the oxidation rate and required longer reaction times. This may be attributed to steric hindrance that impedes oxidation of the bulky substituents of benzylic alcohols (Table 7, entries 8, 14, 15, 19, and 20). Usually, the oxidation of aliphatic alcohols is much more difficult than that of benzylic alcohols.[25d,40] As an example, citronellol, an aliphatic alcohol, exhibited complete conversion in longer reaction time (90 min) compared to benzylic alcohols, which could be attributed to the absence of conjugation in the β-position of the hydroxyl group (Table 7, entry 21).

3. Conclusions

We have reported the synthesis of **ZrO_x-(*x*%)–$MnCO_3$** (where $x = 1–7$%) and **ZrO_x-(*x*%)–Mn_2O_3** ($x = 1–7$%) catalysts for the aerobic oxidation of alcohols. To evaluate the catalytic activities of the as-prepared catalysts, a comparative study of catalytic efficiency between **ZrO_x-(*x*%)–$MnCO_3$** ($x = 1–7$%) and **ZrO_x-(*x*%)–Mn_2O_3** ($x = 1–7$%) oxide along with the effect of zirconia on the catalytic performance was carried out. During this study, it was revealed that **ZrO_x-(1%)–$MnCO_3$** displayed superior performance as compared to its oxide counterpart. Furthermore, it was ascertained that the presence of zirconia enhances the catalytic performance of the catalyst, which yielded 100% conversion to benzaldehyde during the oxidation of benzyl alcohol. The reaction time for this conversion is approximately 5 min with a specific activity of 48.00 mmol$g^{-1}h^{-1}$; these values (best to our knowledge) are among the best for any catalyst reported for the catalytic oxidation of benzyl alcohol. Moreover, the use of molecular O_2 as a source of oxygen makes this catalyst an environmentally friendly catalyst for liquid-phase oxidation of benzylic alcohols. The **ZrO_x-(1%)–$MnCO_3$** catalyst was also tested for various substituted benzylic alcohols, and it is found that 100% conversion products (i.e. corresponding aldehydes) are formed; however, the reaction time varies based on the nature of substituent present on the aromatic ring. Notably, the oxidation of benzylic alcohols that contain electron-withdrawing and bulky groups required longer reaction times than those containing electron-donating groups to the corresponding aldehydes. Furthermore, catalytic performance towards the oxidation of aliphatic alcohol showed that the synthesized catalysts displayed lower conversions for the aliphatic alcohols, which may be attributed to absence of conjugation. These results suggest that the as-prepared catalysts are selective towards the aromatic alcohols. Moreover, the prepared catalyst possesses numerous merits including high conversions, specific activities, and selectivity towards aromatic alcohols and a very short reaction time.

© 2017 The Authors. Published by Wiley-VCH Verlag GmbH & Co. KGaA, Weinheim

Acknowledgements

The authors extend their appreciation to the Deanship of Scientific Research at King Saud University for funding this work through the research group project No. RG-1436-032.

Keywords: benzyl alcohol oxidation · manganese carbonate · manganese oxide · mixed metal oxides · zirconia

[1] C. Zhu, G. Saito, T. Akiyama, *J. Mater. Chem.* **2013**, *1*, 7077 – 7082.
[2] C. A. Antonyraj, J. Jeong, B. Kim, S. Shin, S. Kim, K.-Y. Lee, J. K. Cho, *J. Ind. Eng. Chem.* **2013**, *19*, 1056 – 1059.
[3] C. Santra, M. Pramanik, K. K. Bando, S. Maity, B. Chowdhury, *J. Mol. Catal. A: Chem.* **2016**, *418*, 41 – 53.
[4] a) R. A. Hameed, R. Amin, K. El-Khatib, A. E. Fetohi, *Appl. Surf. Sci.* **2016**, *367*, 382 – 390; b) X. Pan, N. Zhang, X. Fu, Y.-J. Xu, *Appl. Catal. A* **2013**, *453*, 181 – 187.
[5] R. Xie, G. Fan, L. Yang, F. Li, *Chem. Eng. J.* **2016**, *288*, 169 – 178.
[6] a) Q. Wu, C. Zhang, B. Zhang, X. Li, Z. Ying, T. Liu, W. Lin, Y. Yu, H. Cheng, F. Zhao, *J. Colloid Interface Sci.* **2016**, *463*, 75 – 82; b) Y. Goto, K.-i. Shimizu, T. Murayama, W. Ueda, *Appl. Catal. A* **2016**, *509*, 118 – 122; c) J. Yang, M. Cho, Y. Lee, *Biosens. Bioelectron.* **2016**, *75*, 15 – 22; d) F. Neatu, R. S. Marin, M. Florea, N. Petrea, O. D. Pavel, V. I. Pârvulescu, *Appl. Catal. B* **2016**, *180*, 751 – 757.
[7] R. Kannan, A. R. Kim, K. S. Nahm, D. J. Yoo, *Int. J. Hydrogen Energy* **2016**, *41*, 6787 – 6797.
[8] M. Gheju, I. Balcu, G. Mosoarca, *J. Hazard. Mater.* **2016**, *310*, 270 – 277.
[9] M. Fayazi, M. A. Taher, D. Afzali, A. Mostafavi, *Sens. Actuators B* **2016**, *228*, 1 – 9.
[10] a) Y. Tian, Z. Liu, R. Xue, L. Huang, *J. Alloys Compd.* **2016**, *671*, 312 – 317; b) X. L. Guo, M. Kuang, F. Dong, Y. X. Zhang, *Ceram. Int.* **2016**, *42*, 7787 – 7792.
[11] C. Sun, J. Yang, Z. Dai, X. Wang, Y. Zhang, L. Li, P. Chen, W. Huang, X. Dong, *Nano Res.* **2016**, *9*, 1300 – 1309.
[12] L.-Y. Lin, H. Bai, *Chem. Eng. J.* **2016**, *291*, 94 – 105.
[13] a) M. S. Ahmed, D. Park, S. Jeon, *J. Power Sources* **2016**, *308*, 180 – 188; b) M.-Q. Yang, Y.-J. Xu, *Phys. Chem. Chem. Phys.* **2013**, *15*, 19102 – 19118.
[14] T. J. Clarke, T. E. Davies, S. A. Kondrat, S. H. Taylor, *Appl. Catal. B* **2015**, *165*, 222 – 231.
[15] R. Ali, M. Assal, A. Al-Warthan, *Asian J. Chem.* **2013**, *25*, 4815 – 4819.
[16] a) G. Wu, Y. Gao, F. Ma, B. Zheng, L. Liu, H. Sun, W. Wu, *Chem. Eng. J.* **2015**, *271*, 14 – 22; b) H. Einaga, N. Maeda, S. Yamamoto, Y. Teraoka, *Catal. Today* **2015**, *245*, 22 – 27; c) T. J. Clarke, S. A. Kondrat, S. H. Taylor, *Catal. Today* **2015**, *258*, 610 – 615; d) K. A. Castro, S. M. Pires, M. A. Ribeiro, M. M. Simões, M. G. P. Neves, W. H. Schreiner, F. Wypych, J. A. Cavaleiro, S. Nakagaki, *J. Colloid Interface Sci.* **2015**, *450*, 339 – 352; e) S. C. Kim, Y.-K. Park, J. W. Nah, *Powder Technol.* **2014**, *266*, 292 – 298; f) M. Piumetti, D. Fino, N. Russo, *Appl. Catal. B* **2015**, *163*, 277 – 287; g) S.-H. Peng, M. H. Mahmood, H.-B. Zou, S.-B. Yang, H.-Y. Liu, *J. Mol. Catal. A. Chem.* **2014**, *395*, 180 – 185; h) G. Qi, W. Li, *Catal. Today* **2015**, *258*, 205 – 213; i) Q. Tang, X. Gong, P. Zhao, Y. Chen, Y. Yang, *Appl. Catal. A* **2010**, *389*, 101 – 107.
[17] a) Y. Su, L.-C. Wang, Y.-M. Liu, Y. Cao, H.-Y. He, K.-N. Fan, *Catal. Commun.* **2007**, *8*, 2181 – 2185; b) S. Mandal, C. Santra, K. K. Bando, O. O. James, S. Maity, D. Mehta, B. Chowdhury, *J. Mol. Catal. A: Chem.* **2013**, *378*, 47 – 56; c) Y. Guo, J. Zhao, J. Xu, W. Wang, F. Tian, G. Yang, M. Song, *J. Nat. Gas Chem.* **2007**, *16*, 210 – 212; d) S. F. Adil, M. E. Assal, M. Khan, A. Al-Warthan, M. R. H. Siddiqui, *Oxid. Commun.* **2013**, *36*, 778 – 791; e) S. Alabbad, S. Adil, M. Assal, M. Khan, A. Alwarthan, M. R. H. Siddiqui, *Arabian J. Chem.* **2014**, *7*, 1192 – 1198.
[18] R. Bacani, T. S. Martins, M. C. A. Fantini, D. G. Lamas, *J. Alloys Compd.* **2016**, *671*, 396 – 402.
[19] O. H. Laguna, A. Pérez, M. A. Centeno, J. A. Odriozola, *Appl. Catal. B* **2015**, *176 – 177*, 385 – 395.
[20] A. V. H. Soares, J. B. Salazar, D. D. Falcone, F. A. Vasconcellos, R. J. Davis, F. B. Passos, *J. Mol. Catal. A: Chem.* **2016**, *415*, 27 – 36.
[21] S. Farhadi, M. Zaidi, *Appl. Catal. A* **2009**, *354*, 119 – 126.
[22] a) S. Farhadi, Z. Momeni, *J. Mol. Catal. A: Chem.* **2007**, *277*, 47 – 52; b) M. Gruttadauria, L. F. Liotta, G. Deganello, R. Noto, *Tetrahedron* **2003**, *59*, 4997 – 5002; c) T. Yasu-eda, S. Kitamura, N.-o. Ikenaga, T. Miyake, T. Suzuki, *J. Mol. Catal. A: Chem.* **2010**, *323*, 7 – 15; d) T. W. Goh, C. Xiao, R. V. Maligal-Ganesh, X. Li, W. Huang, *Chem. Eng. Sci.* **2015**, *124*, 45 – 51; e) A. R. Hajipour, H. Karimi, *Chin. J. Catal.* **2014**, *35*, 1529 – 1533; f) T. Zhang, Y.-Q. Deng, W.-F. Zhou, C.-T. Au, S.-F. Yin, *Chem. Eng. J.* **2014**, *240*, 509 – 515; g) X. Wang, X. Cao, X. Hu, G. Li, L. Zhu, C. Hu, *J. Mol. Catal. A: Chem.* **2012**, *357*, 1 – 10; h) J. S. Moura, J. d. S. L. Fonseca, N. Bion, F. Epron, T. de Freitas Silva, C. G. Maciel, J. M. Assaf, M. do Carmo Rangel, *Catal. Today* **2014**, *228*, 40 – 50.
[23] T. Sreethawong, S. Ngamsinlapasathian, S. Yoshikawa, *J. Mol. Catal. A: Chem.* **2013**, *374*, 94 – 101.
[24] L. Smoláková, M. Kout, E. Koudelková, L. Čapek, *Ind. Eng. Chem. Res.* **2015**, *54*, 12730 – 12740.
[25] a) P. Cruz, Y. Pérez, I. del Hierro, M. Fajardo, *Microporous Mesoporous Mater.* **2016**, *220*, 136 – 147; b) S. Pathan, A. Patel, *Chem. Eng. J.* **2014**, *243*, 183 – 191; c) M. Forouzani, H. R. Mardani, M. Ziari, A. Malekzadeh, P. Biparva, *Chem. Eng. J.* **2015**, *275*, 220 – 226; d) J. Albadi, A. Alihoseinzadeh, A. Razeghi, *Catal. Commun.* **2014**, *49*, 1 – 5; e) V. Choudhary, D. Dumbre, B. Uphade, V. Narkhede, *J. Mol. Catal. A: Chem.* **2004**, *215*, 129 – 135; f) B. Zahed, H. Hosseini-Monfared, *Appl. Surf. Sci.* **2015**, *328*, 536 – 547; g) C. Ragupathi, J. J. Vijaya, R. T. Kumar, L. J. Kennedy, *J. Mol. Struct.* **2015**, *1079*, 182 – 188; h) C. Ragupathi, J. J. Vijaya, S. Narayanan, S. Jesudoss, L. J. Kennedy, *Ceram. Int.* **2015**, *41*, 2069 – 2080; i) J. Yu, J. Li, H. Wei, J. Zheng, H. Su, X. Wang, *J. Mol. Catal. A: Chem.* **2014**, *395*, 128 – 136; j) Q. Tang, X. Gong, C. Wu, Y. Chen, A. Borgna, Y. Yang, *Catal. Commun.* **2009**, *10*, 1122 – 1126; k) M. Gholizadeh, M. Ebrahimpour, S. F. Hojati, B. Maleki, *Arabian J. Chem.* **2014**, *7*, 267 – 271; l) M. Xie, X. Dai, S. Meng, X. Fu, S. Chen, *Chem. Eng. J.* **2014**, *245*, 107 – 116; m) N. Jamwal, R. K. Sodhi, P. Gupta, S. Paul, *Int. J. Biol. Macromol.* **2011**, *49*, 930 – 935.
[26] F. Z. Su, Y. M. Liu, L. C. Wang, Y. Cao, H. Y. He, K. N. Fan, *Angew. Chem.* **2008**, *120*, 340 – 343.
[27] T. Ishida, R. Takamura, T. Takei, T. Akita, M. Haruta, *Appl. Catal. A* **2012**, *413*, 261 – 266.
[28] a) Y. S. Jun, T. A. Kendall, S. T. Martin, C. M. Friend, J. J. Vlassak, *Environ. Sci. Technol.* **2005**, *39*, 1239 – 1249; b) J. Gao, X. Tong, X. Li, H. Miao, J. Xu, *J. Chem. Technol. Biotechnol.* **2007**, *82*, 620 – 625.
[29] F. Adam, W.-T. Ooi, *Appl. Catal. A* **2012**, *445*, 252 – 260.
[30] R. Ali, S. Adil, A. Al-warthan, M. R. H. Siddiqui, *J. Chem.* **2013**, *2013*; DOI: 10.1155/2013/367261.
[31] M. Zahmakıran, S. Özkar, *Mater. Chem. Phys.* **2010**, *121*, 359 – 363.
[32] Z. Hu, Y. Zhao, J. Liu, J. Wang, B. Zhang, X. Xiang, *J. Colloid Interface Sci.* **2016**, *483*, 26 – 33.
[33] J. Wang, S. A. Kondrat, Y. Wang, G. L. Brett, C. Giles, J. K. Bartley, L. Lu, Q. Liu, C. J. Kiely, G. J. Hutchings, *ACS Catal.* **2015**, *5*, 3575 – 3587.
[34] T. Wang, X. Yuan, S. Li, L. Zeng, J. Gong, *Nanoscale* **2015**, *7*, 7593 – 7602.
[35] H. Wang, W. Fan, Y. He, J. Wang, J. N. Kondo, T. Tatsumi, *J. Catal.* **2013**, *299*, 10 – 19.
[36] A. Aktaş, İ. Acar, E. T. Saka, Z. Biyiklioglu, *J. Organomet. Chem.* **2016**, *815 – 816*, 1 – 7.
[37] E. J. García-Suárez, M. Tristany, A. B. García, V. Collière, K. Philippot, *Microporous Mesoporous Mater.* **2012**, *153*, 155 – 162.
[38] a) Z. Nadealian, V. Mirkhani, B. Yadollahi, M. Moghadam, S. Tangestaninejad, I. Mohammadpoor-Baltork, *J. Coord. Chem.* **2012**, *65*, 1071 – 1081; b) K. P. Peterson, R. C. Larock, *J. Org. Chem.* **1998**, *63*, 3185 – 3189.
[39] a) M. M. Kadam, K. B. Dhopte, N. Jha, V. G. Gaikar, P. R. Nemade, *New J. Chem.* **2016**, *40*, 1436 – 1442; b) M. Heidari-Golafzani, M. Rabbani, R. Rahimi, A. Azad, *RSC Adv.* **2015**, *5*, 99640 – 99645.
[40] a) E. Assady, B. Yadollahi, M. Riahi Farsani, M. Moghadam, *Appl. Organomet. Chem.* **2015**, *29*, 561 – 565; b) S. Hasannia, B. Yadollahi, *Polyhedron* **2015**, *99*, 260 – 265.

Received: September 26, 2016
Published online on December 7, 2016

 © 2017 The Authors. Published by Wiley-VCH Verlag GmbH & Co. KGaA, Weinheim